

Supporting Information

Mapping space charge carrier dynamics in plasmonic-based perovskite solar cells

Shrabani Panigrahi^{*#}, Santanu Jana[#], Tomás Calmeiro, Daniela Nunes, Jonas Deuermeier,
Rodrigo Martins, Elvira Fortunato^{*}

CENIMAT/i3N, Faculdade de Ciências e Tecnologia–Universidade NOVA de Lisboa and
CEMOP/Uninova, Campus de Caparica, 2829-516 Caparica, Portugal.

[#] Authors have equal contribution.

Corresponding Authors

Shrabani Panigrahi - spqdot@gmail.com and Elvira Fortunato - emf@fct.unl.pt

Supporting Figures

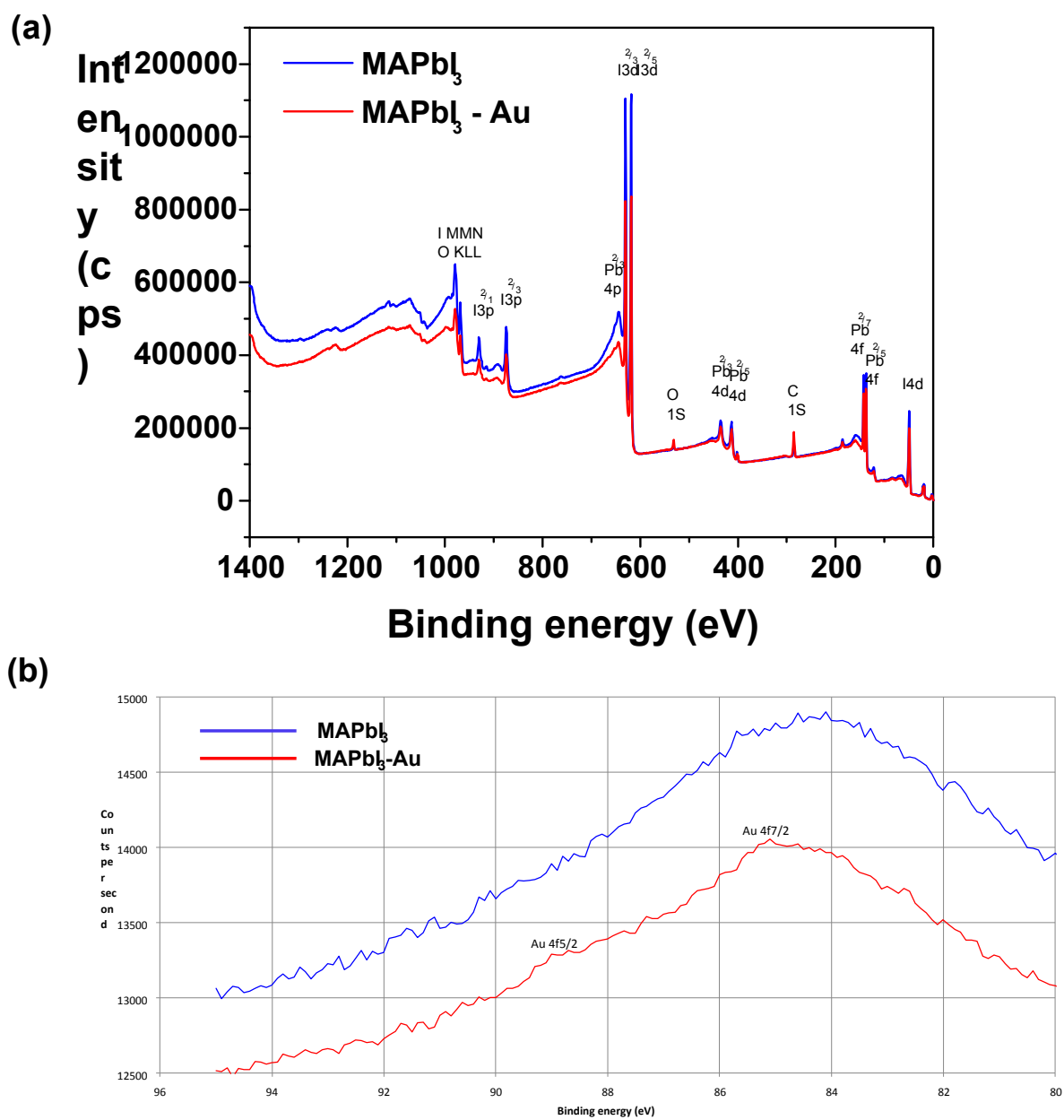


Fig. S1. (a) XPS results of perovskite films before and after plasmonic treatment: MAPbI_3 and $\text{MAPbI}_3\text{-Au}$ film. (b) High resolution XPS data of MAPbI_3 and $\text{MAPbI}_3\text{-Au}$ film which shows very small peak for Au due to presence of very little amount of Au in MAPbI_3 perovskite layer.

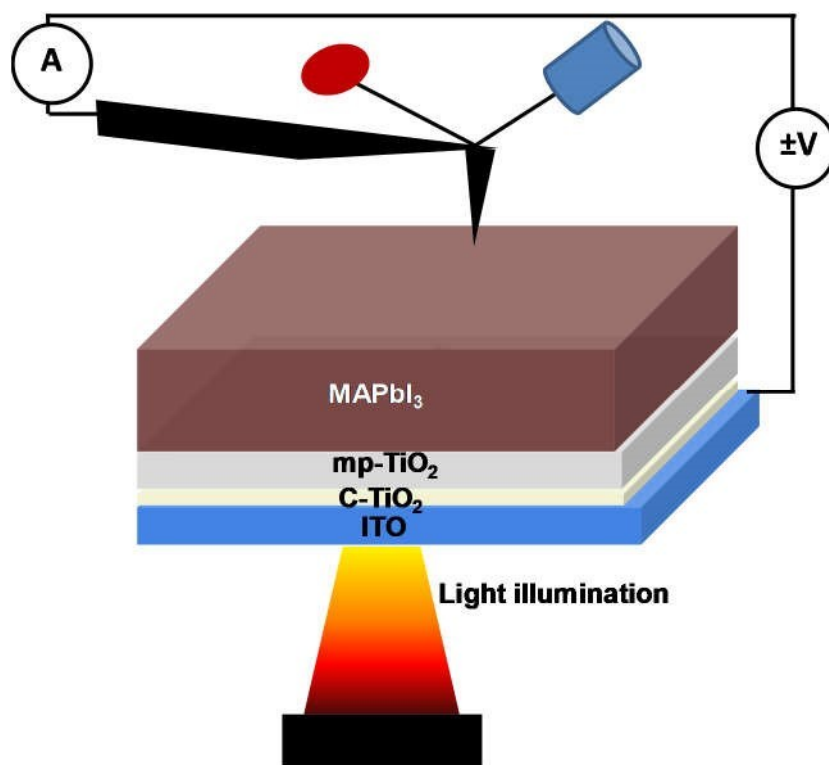


Fig. S2. Schematic diagram of the pc-AFM configuration where the perovskite solar cell is illuminated from below through a transparent-conducting cathode (ITO/glass) while measuring local current with a positionable conductive AFM probe anode from above.

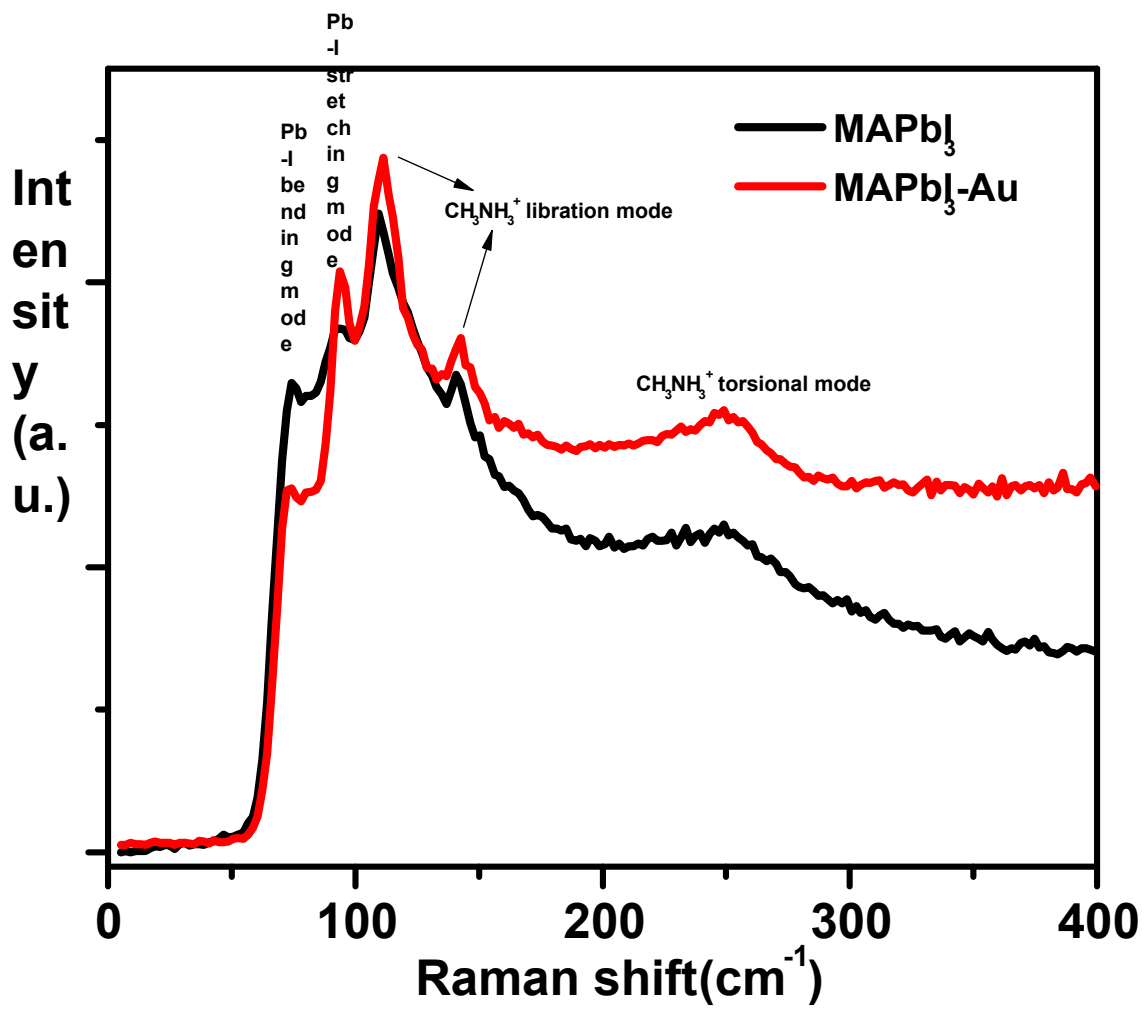


Fig. S3. Raman spectra of the perovskite film before and after plasmonic treatment (MAPbI₃ and MAPbI₃-Au film) under the excitation wavelength of 532 nm.

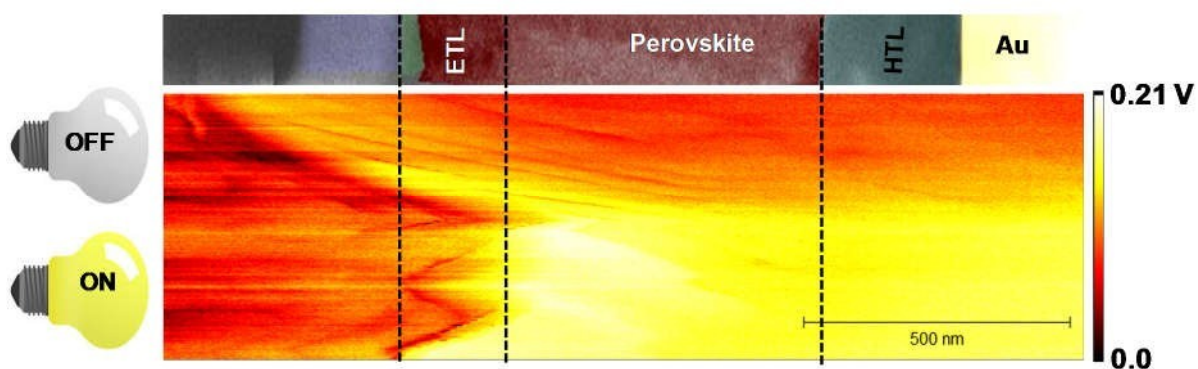


Fig. S4. CPD map across the layers of the cell under dark and illumination condition in a single scan (top: light off and down: light on).

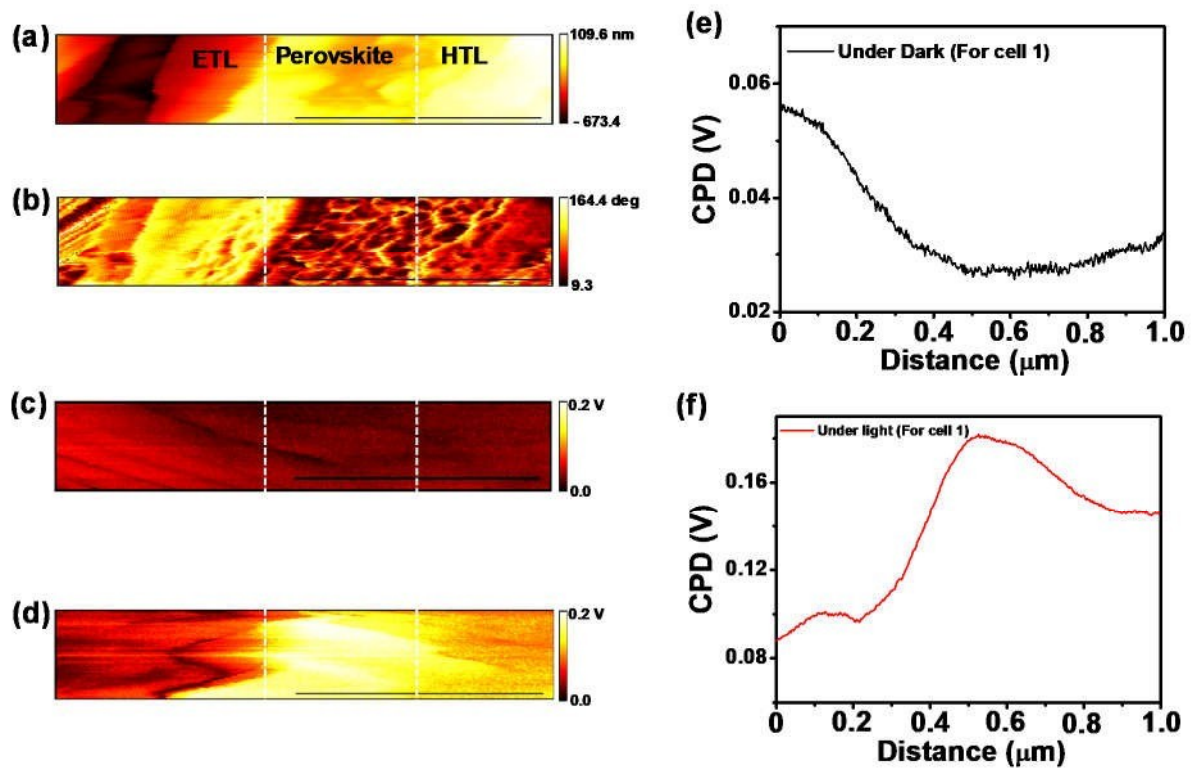


Fig. S5. (a) AFM topography, (b) phase contrast image across the cross section of the solar cell (cell 1). (c), (d) Surface potential images and (e), (f) corresponding potential depth profile across the layers of the solar cell (cell 1) under dark and illumination condition respectively.

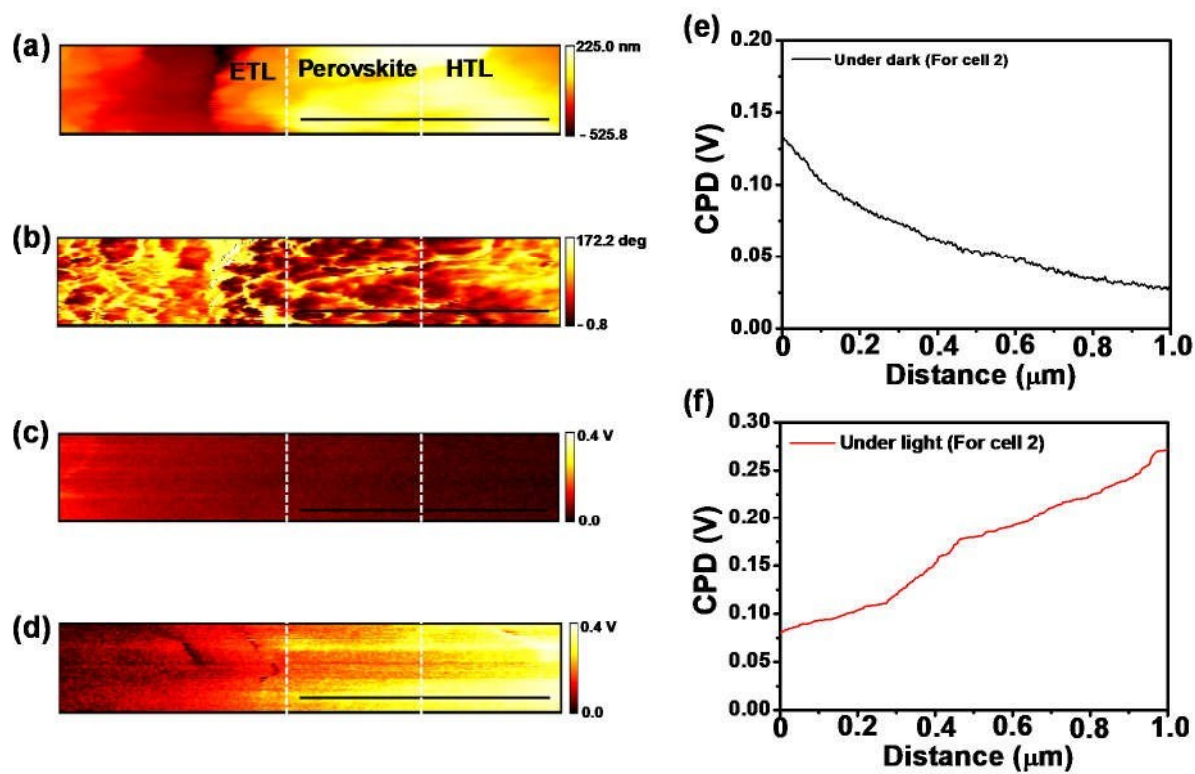


Fig. S6. (a) AFM topography, (b) phase contrast image across the cross section of the solar cell (cell 2). (c), (d) Surface potential images and (e), (f) corresponding potential depth profile across the layers of the solar cell (cell 2) under dark and illumination condition respectively.

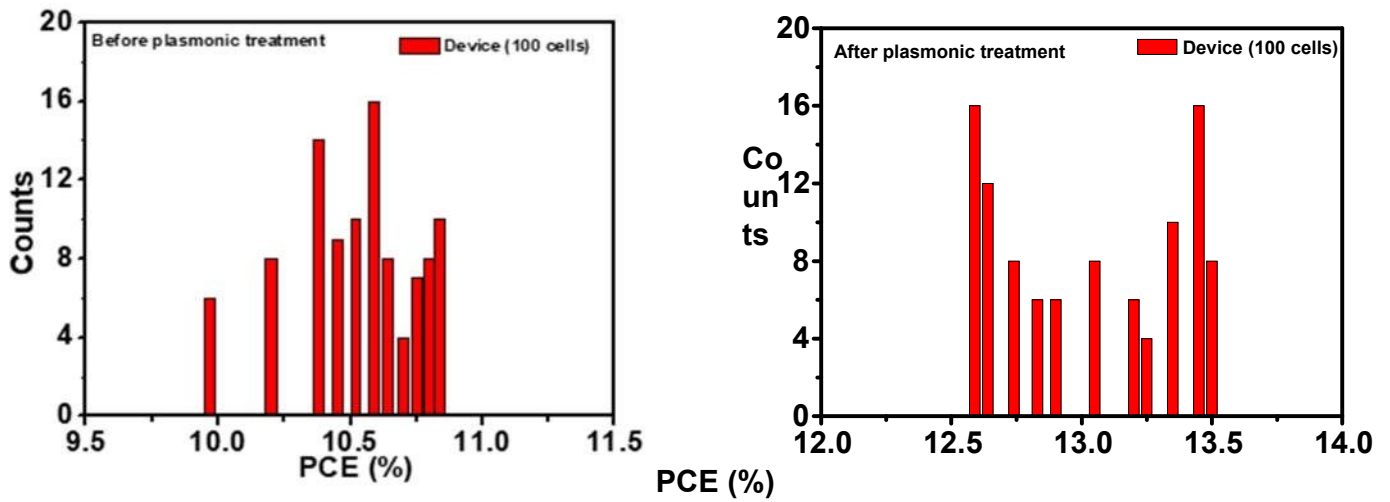


Fig. S7. Efficiency data for 100 cells before and after plasmonic treatment of the devices.

We have observed the current density-voltage (J-V) characteristics for 100 cells before and after plasmonic treatment (Fig. S7). It is obvious that all the cells either before plasmonic treatment or after plasmonic treatment did not show the same efficiency. The efficiency slightly varied from cell to cell but not more than 1%. This efficiency data for 100 cells at before and after plasmonic treatment clearly reveal that the efficiency of the devices are reproducible.

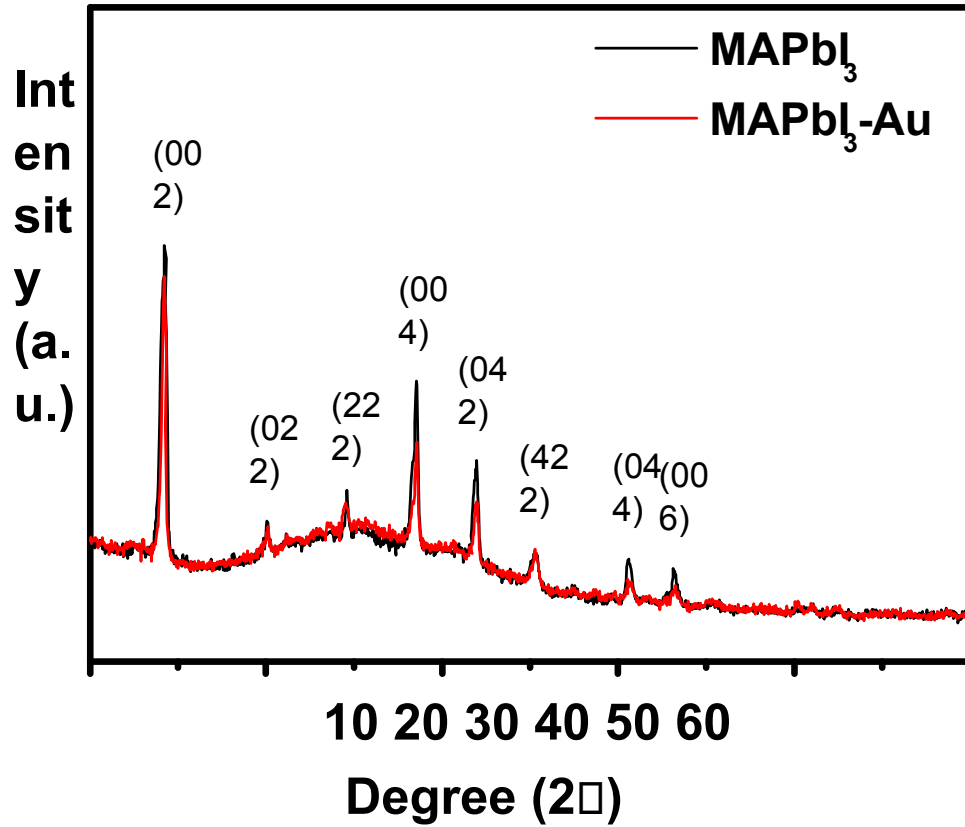


Fig. S8. X-ray diffraction (XRD) pattern of the perovskite film before and after plasmonic treatment.

We have observed X-ray diffraction (XRD) pattern (Fig. S8) of the perovskite film before and after plasmonic treatment. For both cases, the peaks are same without change in FWHM. Therefore, there is no change in crystallinity due to plasmonic treatment. It is clear that inclusion of metal nanoparticles does not change in crystallinity which is contributing to the increase in photoresponse and efficiency.

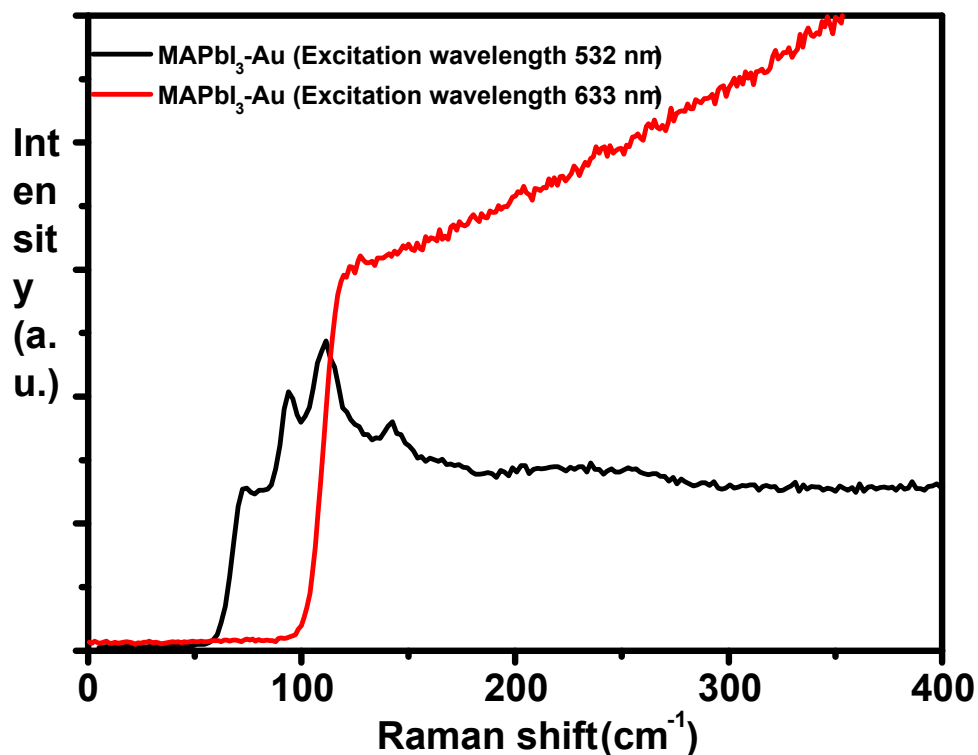


Fig. S9. Raman spectra for MAPbI₃-Au film (after plasmonic treatment) under the excitation wavelength of 532 nm and 633 nm.

We have examined surface-enhanced Raman scattering (SERS) effect of the perovskite layer after the plasmonic treatment with Au NPs for two excitation wavelength 532 and 633 nm. It is clear from the Raman experiment (Fig. S9) that signal for plasmon resonance of Au nanoparticles is observed only for the excitation wavelength 532 nm. There is no peak in Raman spectra when we used the excitation wavelength 633 nm. That means, there is no signal of plasmon resonance of Au nanoparticles.